PHYSICAL REVIEW C **80**, 044302 (2009)

β decay of the proton-rich nucleus ^{24}Si and its mirror asymmetry

Y. Ichikawa,[1,2,*] T. K. Onishi,[1] D. Suzuki,[1] H. Iwasaki,[1] T. Kubo,[2] V. Naik,[3] A. Chakrabarti,[3] N. Aoi,[2] B. A. Brown,[4]
N. Fukuda,[2] S. Kubono,[5] T. Motobayashi,[2] T. Nakabayashi,[6] T. Nakamura,[6] T. Nakao,[1] T. Okumura,[6] H. J. Ong,[7] H. Suzuki,[1]
M. K. Suzuki,[1] T. Teranishi,[8] K. N. Yamada,[2] H. Yamaguchi,[5] and H. Sakurai[1,2]
[1]*Department of Physics, University of Tokyo, 7-3-1 Hongo, Bunkyo, Tokyo 113-0033, Japan*
[2]*RIKEN Nishina Center, RIKEN, 2-1 Hirosawa, Wako, Saitama 351-0198, Japan*
[3]*Variable Energy Cyclotron Centre, 1/AF, Bidhan Nagar, Kolkata-700 064, India*
[4]*Department of Physics and Astronomy, and National Superconducting Cyclotron Laboratory, Michigan State University, East Lansing, Michigan 48824-1321, USA*
[5]*Center for Nuclear Study, University of Tokyo, RIKEN Campus, 2-1 Hirosawa, Wako, Saitama 351-0198, Japan*
[6]*Department of Physics, Tokyo Institute of Technology, 2-12-1 Oh-okayama, Meguro, Tokyo 152-8551, Japan*
[7]*Research Center for Nuclear Physics, Osaka University, 10-1 Mihogaoka, Ibaraki, Osaka 567-0047, Japan*
[8]*Department of Physics, Kyushu University, 6-10-1 Hakozaki, Higashi, Fukuoka 812-8581, Japan*

(Received 26 June 2009; published 5 October 2009)

β-decay spectroscopy of the proton-rich nucleus ^{24}Si was performed. The decay scheme was reconstructed from results of delayed γ-ray and proton measurements. We observed two β branches to bound states in ^{24}Al for the first time. The branching ratios were determined to be 31(4)% and 23.9(15)% for the 1_1^+ state at 0.426 MeV and the state at 1.090 MeV, respectively. The observation of an allowed transition to the 1.090-MeV state enabled us to firmly determine its spin-parity as 1^+. In the proton measurements performed with the ΔE-E method, we observed a new unbound level at 6.735 MeV. The branching ratios to three unbound states, including the new level, were also determined for the first time. Based on the decay scheme, the B(GT) values of ^{24}Si were deduced. The B(GT) values were smaller than those of the mirror nucleus ^{24}Ne by 22% and 10% for the 1_1^+ and 1_2^+ states, respectively. The mirror asymmetries of B(GT), observed in both the 1_1^+ and the 1_2^+ states, indicate changes in configuration in the wave function associated with the Thomas-Ehrman shift. To clarify the mechanism of this asymmetry, a comparison with shell-model calculations is also discussed. The calculations attribute the changes in configuration to the lowering of the $1s_{1/2}$ orbital.

DOI: 10.1103/PhysRevC.80.044302 PACS number(s): 23.40.−s, 23.20.Lv, 23.50.+z, 27.30.+t

I. INTRODUCTION

Mirror symmetry as manifested in energy levels and transitions in conjugate nuclei is a consequence of the charge symmetry of the strong interaction between protons and neutrons. However, it is broken by the Coulomb force acting between protons. In a proton-rich nucleus, the proton separation energy becomes weaker than the neutron separation energy in its mirror nucleus due to the Coulomb potential. Such weakening of the binding energy affects the nuclear structure, especially in nuclei where the outermost proton occupies the $s_{1/2}$ orbital, and can give rise to mirror "asymmetry." One of the important phenomena arising from this kind of mirror asymmetry is the Thomas-Ehrman (TE) shift [1,2].

The TE shift is a reduction of the Coulomb energy caused by the spatial expansion of an s-wave proton, and is important for the spectra of nuclei near the proton drip line. A signature of the TE shift can be found in the spectra of the mirror nuclei ^{17}F and ^{17}O, where the excitation energy of the $1/2^+$ state in ^{17}F is lowered by 375 keV relative to ^{17}O [3]. In addition to the classical interpretation of the TE shift, novel interpretations connected to mirror asymmetry of the configuration in the wave function [4,5] have been suggested. In one such interpretation [5], the TE shift is regarded as lowering of the single particle energy of the $s_{1/2}$ orbital, inducing changes in the configuration in the wave function.

In the lower sd-shell region, the TE shift of the $1s_{1/2}$ orbital relative to the $0d_{5/2}$ orbital results in changes in the valence configurations involving the $1s_{1/2}$ and the $0d_{5/2}$ orbitals in proton-rich nuclei relative to those in their mirror nuclei. These changes in configuration, which involve a weakly bound s-wave proton, could be related to a proton halo structure as postulated for ^{23}Al in order to explain its anomalously large interaction cross section [6]. Although the ground state spin-parity (J^π) of ^{23}Al is $5/2^+$ [7], which implies that the odd proton resides in the $0d_{5/2}$ orbital, the halo structure might be related to an enhanced mixing of configurations involving the $1s_{1/2}$ orbital. Therefore, it is important to investigate the changes in configuration in order to understand the characteristic structure of proton-rich nuclei.

The Gamow-Teller transition strength B(GT) provides a means for exploring the effects of the changes in configuration caused by the TE shift. B(GT) is defined as the square of the matrix element, where the GT operator $\sigma\tau$ was taken between the initial state $|i\rangle$ and the final state $|f\rangle$, as $B(\mathrm{GT}) = \langle f|\sigma\tau|i\rangle^2$. Since $\sigma\tau$ changes only the quantum numbers of the spin and the isospin, B(GT) reflects the spatial overlap between the initial and the final wave functions. Thus, by comparing the B(GT) for mirror GT transitions, changes in the

---

[*] ichikawa@ribf.riken.jp; present address: RIKEN Nishina Center, RIKEN, 2-1 Hirosawa, Wako, Saitama 351-0198, Japan.

configuration of a proton-rich nucleus due to a weakly bound s-wave proton would be reflected in a mirror asymmetry of B(GT). In fact, mirror asymmetries of the transition strength have been reported for the β decay of ^{13}O [8] and for the first-forbidden transition of the ground state ^{17}Ne [9] to the $1/2^+$ state in ^{17}F, where the TE shifts are observed.

The structure of the proton-rich nucleus ^{24}Al with isospin $T_z = -1$ provides an important insight into the possible changes in configuration mixing related to weakly bound s-wave protons. A simple shell model yields a picture where ^{24}Al has five valence protons in the $d_{5/2}$ orbital. Thus, a state dominated by s-wave protons is expected to appear in an excited state. In odd-odd $T_z = \pm 1$ nuclei, such as ^{24}Al, the proton-neutron pair can couple to form states with $J^\pi = 1^+$. Figure 1 shows a comparison of the energy levels for the 1^+ states in the mirror pair of ^{24}Al and ^{24}Na. The first 1^+ state is an isomeric state [10]. J^π of the state at 1.111 MeV has been tentatively assigned to (1^+, 2^+, 3^+) [11,12]. Here, J^π of the 1.111 MeV in ^{24}Al is tentatively assumed to be 1^+ based on the existence of a level at 1.346 MeV in ^{24}Na. It is noteworthy that while the energy difference between the first 1^+ states is only 46 keV, the excitation energy of the second 1^+ state in ^{24}Al is lower than the one in ^{24}Na by 235 keV. This energy lowering in the 1_2^+ state in ^{24}Al suggests a TE-type mirror asymmetry, i.e., possible changes in configuration for the bound states of ^{24}Al in connection with the anomalously large interaction cross-section reported for the neighboring ^{23}Al.

GT transition strengths for β decay of ^{24}Si [15] with isospin $T_z = -2$ provide information on the configuration of the 1^+ states in ^{24}Al. Thus far, no experimental studies have been reported for the β decay to the low-lying bound 1^+ states. Regarding β decay to proton-unbound states, several studies have been reported [16–19]. In the most recent study [19], the ΔE-E method was employed to separate the β-delayed protons from the β rays, allowing for the identification of new peaks which could not be identified in earlier work using the implantation method [18]. However, the measurements in [19] provided only the relative intensities and not the absolute branching ratios. In addition, the origins of these new peaks could not be firmly identified due to the low statistics. Therefore, it is necessary to identify the origin of the delayed protons to enable the reconstruction of the entire decay scheme for ^{24}Si with the absolute branching ratio for both the unbound states and the bound states.

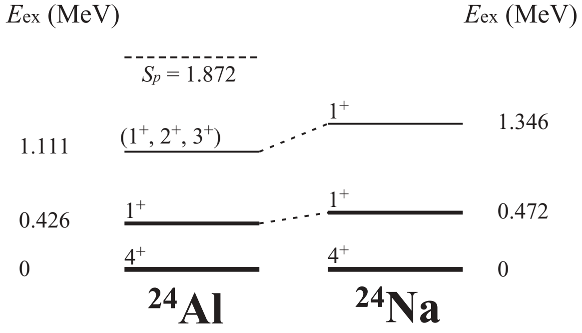

FIG. 1. Comparison of energy levels in $T_z = \pm 1$ $A = 24$ mirror nuclei ^{24}Al and ^{24}Na. Data for ^{24}Al and ^{24}Na are taken from [10–12] and [13], respectively. J^π of the 1.11-MeV level was tentatively assigned to (1^+, 2^+, 3^+) [11,12]. The proton separation energy for ^{24}Al is $S_p = 1.872$ MeV, while neutron separation energy for ^{24}Na is $S_n = 6.959$ MeV [14].

We have performed β-decay spectroscopy of ^{24}Si with measurements of the β-delayed γ rays from particle-bound states and the β-delayed protons from proton-unbound states in ^{24}Al. The entire decay scheme of ^{24}Si is reconstructed by combining the two measurements, and the absolute values of the branching ratio to bound states are determined from the γ-ray measurements. For the proton measurements, the ΔE-E method was employed. We aimed to obtain higher statistics than obtained in previous studies [19] in order to identify the origin of delayed protons. For that purpose, the ΔE-E method was upgraded to cover a larger solid angle, and the number of detectors was increased fourfold. The absolute branching ratios to unbound states are renormalized by taking into account the branching ratios to bound states. The overall B(GT) distribution covering the unbound states is used to understand in greater detail the mechanism of asymmetry through comparison with theoretical calculations.

In this paper, we present the results of β-decay spectroscopy of ^{24}Si. The paper is organized as follows. The details of the experiment are described in Sec. II. Through the analysis described in Sec. III, the decay scheme of ^{24}Si is reconstructed as shown in Sec. IV. A discussion on the B(GT) asymmetry is presented in Sec. V. Finally, a summary is given in Sec. VI.

II. EXPERIMENT

A. Secondary beams

The experiment was performed at the RIKEN Projectile Fragment Separator (RIPS) facility [20]. The secondary beam of ^{24}Si was produced by projectile fragmentation of a 100-MeV/nucleon ^{28}Si beam. As production targets, we used a ^{9}Be target with a thickness of 3.0 mm and a $^{\mathrm{nat}}$Ni target with a thickness of 0.72 mm for the proton and γ-ray measurements. The former was the optimal choice in terms of the yield of ^{24}Si, while the latter provided higher purity. The reaction fragments were collected and analyzed at RIPS. An aluminum wedge degrader with a mean thickness of 221 mg/cm^2 was placed at the momentum dispersive focus (F1) for isotope separation. The momentum acceptance of RIPS was set to $\pm 0.33\%$.

Particle identification of the secondary beam was performed on an event-by-event basis with information regarding time of flight (TOF) and energy loss (ΔE). The TOF was measured using two plastic scintillators, each with a thickness of 0.1 mm, placed at the focal planes of F2 and F3. The ΔE was determined from a silicon detector with a thickness of 100 μm placed at F3. The total intensity of the secondary beam and the purity of ^{24}Si at F3 were 20 (4) kilo per second (kcps) and 1.5 (4.1)%, respectively, with the ^{9}Be ($^{\mathrm{nat}}$Ni) target. The other main contaminants in the secondary beam were $N = 10$ isotones, namely, ^{23}Al, ^{22}Mg and ^{21}Na. The beam was pulsed in order to measure the half-lives through the detection of β-delayed particles. The durations of the beam-on

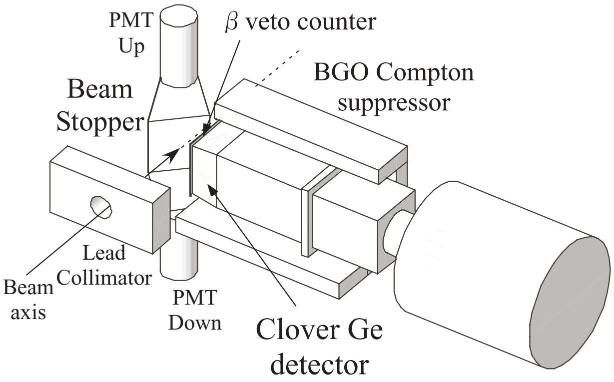

FIG. 2. Schematic view of the setup for γ-ray measurements.

and beam-off periods were chosen to be 500 ms and 500 ms, respectively. A ^{21}Mg beam was also produced at RIPS for the purpose of calibrating the detectors used in the delayed proton measurements.

B. Setup for delayed γ rays

The γ-ray setup consisted of an active beam stopper, a clover-type Ge detector equipped with BGO Compton suppressors, and a plastic β-veto counter, as shown in Fig. 2. The radioactive ions were implanted into the active stopper to count the number of implanted ions and to determine the absolute branching ratio. We employed for the active stopper a plastic scintillator with a thickness of 5 mm and an area of 100 × 100 mm^2 coupled with photomultiplier tubes (PMTs) at both ends. The coincidence of signals from the two PMTs allowed us to detect implanted ions as well as β rays emitted from the ions. The stopper was tilted at an angle of 45 degrees with respect to the beam axis. A lead collimator with a hole of 40 mm ϕ was set 16.0 cm upstream from the stopper in such a way that nuclei were implanted only in the central region of the stopper. To monitor the transmission through the collimator and to determine the distribution of the beam position on the stopper, which can affect the detection efficiency, the beam profile was measured with two position-sensitive detectors (PPACs [21]) at F3.

The delayed γ rays were detected using the Ge detector placed 6.0 cm apart from the center of the stopper. Standard sources ^{152}Eu, ^{60}Co, and ^{56}Co were used for energy calibration and detection efficiency measurements. The energy resolution was measured to be 2 keV in FWHM for 1.3-MeV γ rays. In this geometry, γ rays from nuclei stopped in the collimator were hardly detectable with the Ge detector, which was also confirmed using the sources attached in the collimator. Eight BGO counters surrounded the Ge detector in order to suppress continuum-γ backgrounds deriving from Compton scattering. Each BGO counter had a size of 30 × 80 × 250 mm^3. A plastic β-veto counter with a thickness of 1 mm and an area of 100 × 100 mm^2 was placed in front of the Ge detector to reject β rays incident to the detector. The BGO and β-veto counters allowed us to improve the signal-to-background ratio.

The data acquisition system was triggered by a γ-hit event defined by a logical OR of signals from the crystals of the clover Ge detector. The timing of each γ event was determined from the start timing of the beam-on period in order to obtain the decay curve and to determine the half-life of the decay. The shape of the decay curves can be distorted by the dependence of the dead-time on the trigger rate. Thus, random pulses generated from cosmic rays incident to an ancillary plastic scintillator were mixed with the trigger in order to deduce the dead-time and used to correct the distortion in the decay curves.

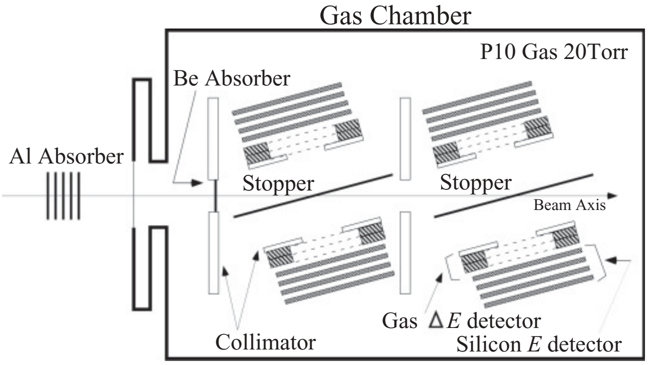

FIG. 3. Schematic view of the setup for proton measurements.

C. Setup for delayed protons

In the proton measurements, we employed the ΔE-E method, which allowed us to identify delayed protons and to reject β rays. A schematic view of the setup is shown in Fig. 3. The detector systems were placed in a chamber filled with a 20-Torr P10 (Ar 90% + CH$_4$ 10%) gas. In the gas chamber, two Al stopper foils were placed at an angle of 15 degrees with respect to the beam axis. Energy straggling and fluctuations in the energy loss due to differences in trajectory in the stopper cause the deterioration of the energy resolution. To suppress the effect, we used Al foils which were as thin as 2.8 μm. The effective thickness of the two stopper foils amounted to 20 μm along the beam axis.

The stopping range of the ^{24}Si beam was adjusted by using two energy absorbers in such a way that the beam stops in the two Al stopper foils. One of the absorbers was a variable energy absorber placed in front of the chamber which was in the form of a stack of Al foils. The other one was a Be absorber with a thickness of 5 mm placed inside the chamber, because multiple scatterings were smaller for Be than for higher materials. For the range adjustment, an silicon detector with a thickness of 500 μm was inserted temporarily behind the Be absorber. The range adjustment was performed by using information of the transmission between the silicon detectors at the F3 focal plane and the one inside the chamber. As a result of the range adjustment, the thickness of the variable Al absorber was set to 830 μm. The silicon detector in the chamber was removed before the measurements.

Delayed protons emitted from ^{24}Si in the Al stoppers were detected using four ΔE-E telescopes placed on both sides of the stoppers at a distance of 2.5–4.0 cm. Each ΔE-E telescope was composed of gas ΔE [22] and silicon E detectors. The gas ΔE detector consists of three electrodes made of a wire-mesh sheet with an area of 50 × 50 mm^2 and a transmission factor of 95%. The center electrode was used as an anode, while those at both ends were connected to the ground. The interelectrode gap was 3 mm on either side of the anode. The anode voltage was maintained at 300 V, which allowed operation in the proportional region. A performance test using an α source (^{241}Am) was used in order to ensure that the ΔE detectors did not exhibit a dependence on the position with respect to the detection efficiency. Four silicon E detectors, each with a thickness of 450 μm and an area of 50×50 mm^2, were placed behind each ΔE detector to measure the energy of protons up to 18 MeV. A stainless steel collimator with a thickness of 2 mm and a diameter of 30 mm was attached to the front face of each gas ΔE detector in order to limit the trajectory of the protons and to suppress the deterioration of the energy resolution. The solid angle acceptance of the ΔE-E telescope was improved to cover a region approximately three times larger than that in the previous experiment [19].

The data acquisition system was triggered by a single proton-hit event defined by a logical OR of signals from the first layers of the silicon E detectors. As in the case of the γ-ray measurements, the time of each proton event was recorded in order to obtain the decay curve. A random trigger was also mixed with the trigger for the dead-time correction.

III. DATA ANALYSIS

In this section, analysis procedures for the delayed γ rays and protons are described. The objectives of the γ-ray analysis were to identify delayed γ rays of ^{24}Si and to obtain the γ-line yields and the detection efficiency for the deduction of the absolute branching ratio. In the proton analysis, we identified the delayed protons of ^{24}Si in the proton energy spectrum through proton-β separation performed with the ΔE-E method, after which we derived the relative intensities for the protons.

A. Analysis for delayed γ rays

To identify delayed γ rays of ^{24}Si and to obtain those yields, the following two energy spectra for γ rays were obtained: a γ-ray singles spectrum with the Ge trigger only, and a spectrum gated by β-γ coincidence, and BGO and β vetoes. Figure 4 shows the γ-ray singles and the gated spectra. In the γ-ray singles spectrum, a γ line of 0.426 MeV from an isomeric state in ^{24}Al [10] was clearly observed, while not in the gated spectrum since the decay of the isomeric state was not accompanied by β-ray emission. The β-γ coincidence allowed us to reject prompt γ rays and backgrounds as well. Hence, γ lines observed in the gated spectrum were derived from β decays. The gated spectrum with a good signal-to-background ratio was used for the identification of γ lines in terms of the half-life associated with each γ line. After the identification, the γ-line yields were counted according to the γ-ray singles spectrum.

The γ lines shown in the gated spectrum were identified in terms of energy. There are four candidates for the delayed γ rays of ^{24}Si, namely, the 0.426-, 0.664-, 1.906-, and 2.357-MeV lines, which are clearly seen in Fig. 4. According to the known low-lying level scheme in ^{24}Al shown in Fig. 1, the 0.426- and 0.664-MeV γ lines correspond to the de-excitations from the bound states of ^{24}Al. The 1.906- and 2.357-MeV γ lines correspond to the de-excitations from the 2.357-MeV level in ^{23}Mg produced by the β-proton decay of ^{24}Si as discussed in previous studies [18,19]. Other γ lines are attributed to delayed γ rays from $N = 10$ isotones.

To confirm the origin of the four γ rays, the half-lives associated with the γ rays were deduced from the decay curve spectra synchronized with the beam pulsing. The decay curve spectra, which are plots of the γ-line yields as a function of time, are demonstrated in Fig 5. The spectrum for the 0.664-MeV γ rays was obtained by gating with an energy window of $\pm 3\sigma$ in the gated energy spectrum, where σ is the energy resolution in rms. A typical value of σ is 1.6 keV at 0.664 MeV. Dead-time correction was performed by using randomly triggered data. The decay curve was fitted to the function of Eq. (A1) in [23], and the half-life associated with the 0.664-MeV γ ray was determined to be 140.1(26) ms, which is in good agreement with the previous values of the half-life of ^{24}Si, 140(8) ms [18] and 139(18) ms [19]. Thus, it was confirmed that the 0.664-MeV γ rays originate from ^{24}Si. Regarding the 1.906- and 2.357-MeV γ rays, their decay curve spectra were combined due to the low statistics. It should be noted that both γ rays are emitted from the same initial state of 2.357 MeV in ^{23}Mg [24]. Hence, a single common half-life is deduced from the combined spectrum. The half-life for the 1.906- and the 2.357-MeV γ rays was determined to be 139(11) ms, which is also in good agreement with the half-life of ^{24}Si. These two γ rays were also identified as originating from the β-proton decay of ^{24}Si. All four γ rays were observed for the first time as delayed γ rays of ^{24}Si. The results are summarized in Table I. Table I also shows the results for the 0.451-, 1.600-, 2.051-, 2.452-, and 2.903-MeV γ rays from ^{23}Al decay [26,27].

The detection efficiency was deduced on the basis of the measurements of ^{22}Mg decay, whose branching ratios for the 0.583- and 1.280-MeV γ rays were determined with a high degree of certainty in an earlier study [28]. In this case, the energy dependence of the intrinsic efficiency and beam-position dependence of the solid-angle acceptance were considered. The energy dependence was determined using standard sources of ^{152}Eu and ^{56}Co. The position dependence was corrected by performing a Monte Carlo simulation with the GEANT platform [29]. In this simulation, we employed the measured distributions of the beam position on the active stopper, which were determined through the extrapolation of two PPACs [21] at F3. Taking into account the position dependence as obtained from the simulation, we confirmed that the efficiencies for the 0.351-MeV γ ray from ^{21}Na [30] decay were reproduced sufficiently well, with an error of 3%. The error for the simulation stems from the uncertainty of the position distributions. The efficiencies for the 0.426- and 0.664-MeV γ rays were estimated to be 1.35(8)% and 0.92(6)%, respectively.

B. Analysis for delayed protons

The energy of the delayed protons was determined from the possible energy loss at the Al stopper foil and the measured

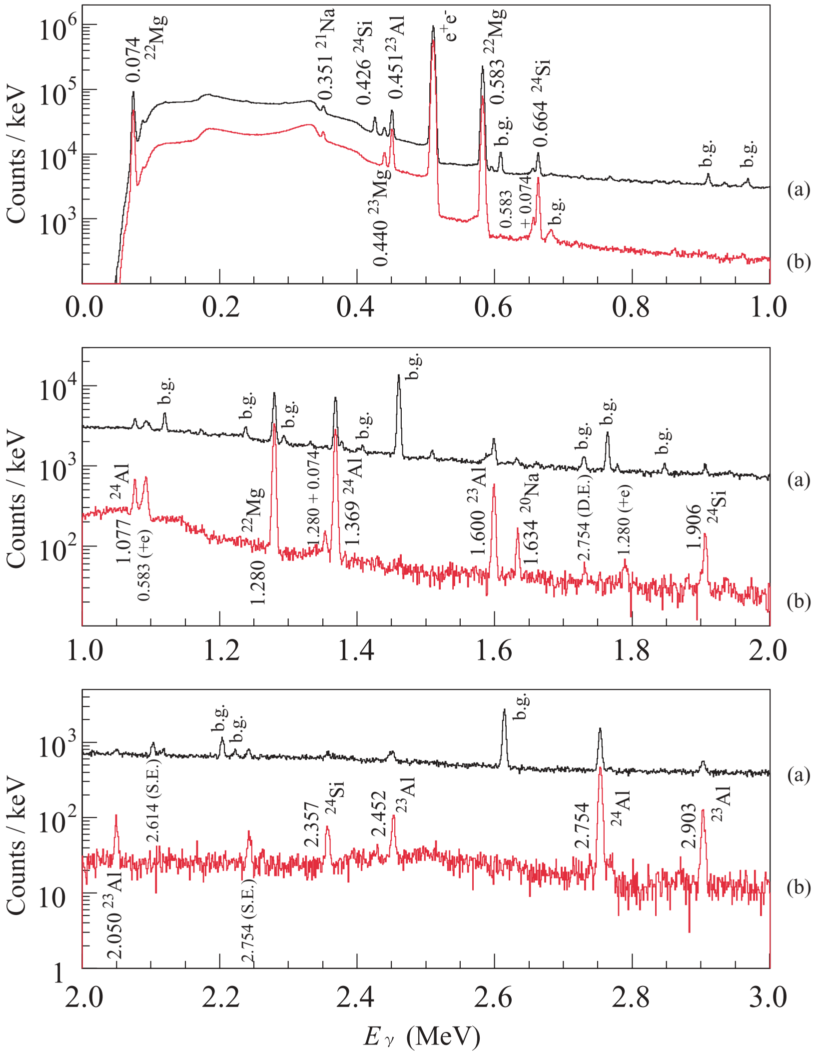

FIG. 4. (Color online) Energy spectrum for γ rays. The black line (a) and the red line (b) represents γ-ray singles spectrum and the spectrum gated by conditions of β-γ coincidence, and BGO and β shield vetoes, respectively. For each observed γ line, its energy E_γ is denoted together with its assumed parent nucleus. Background γ lines from natural sources are denoted by "b.g.", and γ lines caused by single escape, double escape of 0.511-MeV γ rays and by coincidence with them are denoted by "S.E.", "D.E" and "+e", respectively.

energy in the silicon E detectors. The energy loss at the gas is a few tens of keV for 1-MeV protons, which is negligibly smaller than that at the foil (100 keV). Thus, the energy measured at the silicon detector (E_{Si}) is given as $E_{\mathrm{Si}} = E_p - \epsilon E_p^{1-\gamma}$, where E_p is the true proton energy and the second term denotes the energy loss in the Al foil. γ in the second term is a parameter specific to the material, and its value is 1.75 for aluminum. Since ϵ is a small coefficient,

TABLE I. Observed γ rays and their origins. References for γ-ray energy were taken from the table of isotopes [25]. Known de-excitations are shown together with the spin-parity J^π and the energy level E of the initial and final states. Origins of delayed γ rays as identified from their half-lives $T_{1/2}$ are shown in the "Parent" column.

E_γ (MeV)	E_γ [25] (MeV)	Nucleus	J_i^π	E_i [25] (MeV)	J_f^π	E_f [25] (MeV)	$T_{1/2}$ (ms)	Parent
0.664(1)							140.1(26)	^{24}Si
0.426(1)	0.4258(1)	^{24}Al	1^+	0.426	4^+	0		
0.451(1)	0.45070(15)	^{23}Mg	$5/2^+$	0.451	$3/2^+$	0	428(17)	^{23}Al
1.600(1)	1.600(2)	^{23}Mg	$7/2^+$	2.051	$5/2^+$	0.451	325(23)	^{23}Al
2.051(1)	2.051(2)	^{23}Mg	$7/2^+$	2.051	$3/2^+$	0	325(23)	^{23}Al
1.906(1)	1.908(2)	^{23}Mg	$1/2^+$	2.359	$5/2^+$	0.451	139(11)	^{24}Si
2.357(2)	2.359(2)	^{23}Mg	$1/2^+$	2.359	$3/2^+$	0	139(11)	^{24}Si
2.452(2)	2.457(3)	^{23}Mg	$(3/2^+, 5/2^+)$	2.908	$5/2^+$	0.451	314(36)	^{23}Al
2.903(2)	2.908(3)	^{23}Mg	$(3/2^+, 5/2^+)$	2.908	4^+	0	314(36)	^{23}Al

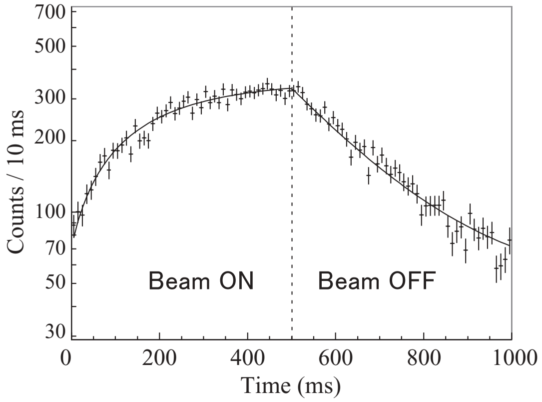

FIG. 5. Decay-curve spectrum for 0.664-MeV γ ray. The decay curve was fitted to the function of Eq. (A1) in [23]. Then, the half-life was determined to be 140.1(26) ms.

E_p in the second term is approximated to be E_{Si}. Therefore, E_p is eventually given as $E_{\mathrm{Si}} + \epsilon E_{\mathrm{Si}}^{1-\gamma}$. The parameters for the channel-to-energy relation and ϵ were determined using the data for the well-known delayed proton emitter ^{21}Mg [31], and therefore the energy calibration of E detectors and the determination of ϵ were performed simultaneously. Furthermore, the inhomogeneity of the detection efficiency at the ΔE-E detectors was also examined with the ^{21}Mg data, which was 5% mainly due to the uncertainty associated with the reference values of ^{21}Mg.

The ΔE-E detectors allowed us to clearly separate the delayed protons of ^{24}Si from β rays in a two-dimensional plot of ΔE-E, as shown in Fig. 6. The separated β rays have a time structure with a half-life of 5 s, and thus the main source of β rays is supposed to be ^{22}Mg with a half-life of 3.9 s stopped at the Al foils and the energy absorbers. The proton energy spectrum shown in Fig. 7 is a one-dimensional projection for protons gated in the window shown in Fig. 6. In Fig. 7, the peaks labeled as 1–13 and Al1, Al2 are clearly seen. All peaks (except for 13) have already been observed in a previous experiment [19]. Peaks Al1 and Al2 are due to delayed protons of ^{23}Al, which are known from earlier studies [27,32]. The peak labeled with *1 is discussed later.

The obtained spectrum contains proton peaks and a background component. The background arises from a slight admixture of a large number of β rays from various sources, such as ^{22}Mg. The proton energy spectrum was simultaneously fitted to 15 Gaussian functions for peaks 1–13 as well as peaks Al1 and Al2 and an exponential function for the background component in order to deduce the proton energies and yields. The relative intensities for the delayed protons were deduced based on an intensity of 100 for peak 10 by taking into account the homogeneous detection efficiency of the ΔE-E detectors. The energies and the relative intensities of the delayed protons are summarized in Table II where they are compared to the results from [18,19]. The uncertainty for the relative intensity shows both statistical and systematical errors. The systematical error is 1%, which corresponds to the uncertainty of the background level. The statistical error includes an error contributable to the deviation of the plot shape from a Gaussian.

The energies and the relative intensities for the delayed protons were compared with those from previous experiments [18,19], as shown in Table II. The relative intensities for peaks 1–12 are reasonably consistent with those obtained in the previous studies [18,19]. The significance of peak 13 is at the 5σ level, and we concluded that peak 13 is a delayed proton peak. Namely, we observed 4.66-MeV protons for the first time.

The origins of the observed protons were confirmed from the half-life associated with each proton peak. To deduce the half-lives, the decay curve for each peak was fitted to a function composed of an exponential form and a constant term. The constant term represents the time structure of the background component. This is necessary since the β rays, which are assumed to cause the background component, have a half-life which is sufficiently longer than that of ^{24}Si. The constant term was a free parameter whose upper and lower limits were obtained from the signal-to-background ratio in the energy spectrum. The deduced half-lives $T_{1/2}$ are shown in Table II. The half lives for peaks 1–12 are in good agreement with the known half-life of ^{24}Si [18,19], which is measured as 140(8) ms [18] and 139(18) ms [19]. Therefore, it was confirmed that peaks 1–12, which have been previously observed, are delayed protons of ^{24}Si. Peak 13 also has a decaying structure with half-life $T_{1/2} = 109(48)$ ms, which is consistent with ^{24}Si, suggesting that peak 13 originates from delayed protons of ^{24}Si. The half-life of ^{24}Si is determined to be $T_{1/2} = 140.8(18)$ ms from the decay spectrum summed for all proton peaks 1–13. A similar analysis was performed for peaks Al1 and Al2, after which these were confirmed to be delayed protons of ^{23}Al which are known from earlier studies [27,32]. The *1 peak seen in Fig. 7 does not have a decaying time structure with the half-life of ^{24}Si. Therefore, it was not identified as corresponding to delayed protons of ^{24}Si.

IV. RESULTS

The entire decay scheme of ^{24}Si was reconstructed by combining the results from the delayed γ-ray and proton measurements. Using the branching ratios and the half-life of ^{24}Si, the *ft* values and the Gamow-Teller transition strengths B(GT) were deduced.

A. Decay scheme of ^{24}Si

In the γ-ray measurements, we observed four ^{24}Si-originating γ rays of 0.426, 0.664, 1.906, and 2.357 MeV for the first time. The 0.426-MeV γ ray corresponds to de-excitation from the 1_1^+ isomeric state [10] to the ground state (g.s.) in ^{24}Al. The 1.906- and 2.357-MeV γ rays are de-excitation γ rays in ^{23}Mg, which is the β-proton daughter of ^{24}Si. The 0.664-MeV γ ray is attributed to de-excitation from the 1.090(1) MeV level to the 1_1^+ state in ^{24}Al. In earlier studies [11,12] using (p,n) or $(^3\mathrm{He},t)$ reactions, the 1.090(1)-MeV level was observed at 1.111(3) MeV and tentatively assigned a spin-parity of the state to $(1^+, 2^+, 3^+)$. The present experiment using β decay has an advantage in terms of the accuracy of

TABLE II. Delayed protons of ^{24}Si with proton energy E_p, total decay energy E_μ, half-life $T_{1/2}$, relative intensity Y and absolute branching ratio b_{i}. Energies of the initial states $E_{\mathrm{ex,i}}$ in ^{24}Al and the final states $E_{\mathrm{ex,f}}$ in ^{23}Mg are also shown. Y were normalized based on an intensity of 100 for the peak 10. References for E_p and Y are taken from Refs. [18,19].

Peak	E_p (MeV)	E_p [18] (MeV)	E_p [19] (MeV)	E_μ (MeV)	$T_{1/2}$ (ms)	Y	Y [18]	Y [19]	b_i (%)	$E_{\mathrm{ex},i}$ (MeV)	$E_{\mathrm{ex},f}$ (MeV)
1	1.072(20)	1.08(3)	1.09	1.119(21)	149(5)	94.6(28)	77.2(60)	75.4(67)	7.5(7)	2.991(21)	0
2	1.430(12)	1.44(3)	1.44	1.492(13)	148(3)	178.5(46)	168.7(121)	144.0(94)	14(1)	3.364(13)	0
3	1.652(12)	1.66(3)	1.66	1.724(13)	132(5)	61.0(21)	82.9(61)	62.6(62)	4.8(5)	5.953(8)	2.357
4	1.940(10)	1.94(5)	1.97	2.024(10)	118(12)	12.7(8)	18.8(61)	10.3(25)	1.0(1)	6.243(12)	2.357
5	2.412(9)	2.41(5)	2.42	2.517(9)	133(11)	7.9(6)	12.7(16)	13.4(29)	0.62(8)	4.389(10)	0
6	2.710(7)	2.71(4)	2.68	2.828(7)	139(8)	17.5(10)	19.8(23)	18.2(33)	1.4(2)	4.700(8)	0
7	2.975(8)	2.97(4)	2.97	3.104(8)	135(9)	12.9(8)	19.0(23)	17.0(32)	1.0(1)	4.976(9)	0
8	3.364(10)		3.42	3.510(10)	138(9)	11.0(8)		6.6(20)	0.87(10)	5.382(11)	0
9	3.765(50)		3.73	3.929(50)	134(7)	16.2(49)		9.1(24)	1.3(4)	5.801(50)	0
10	3.911(7)	3.92(2)	3.92	4.081(7)	141(3)	100	100	100	7.9(8)	5.953(8)	0
11	4.188(11)	4.21(4)	4.19	4.371(11)	141(7)	22.5(11)	35.1(33)	33.4(45)	1.8(2)	6.243(12)	0
12	4.423(11)		4.47	4.615(11)	149(49)	4.2(5)		4.2(16)	0.33(5)	6.487(12)	0
13	4.660(11)			4.863(11)	109(48)	1.1(2)			0.09(2)	6.735(12)	0

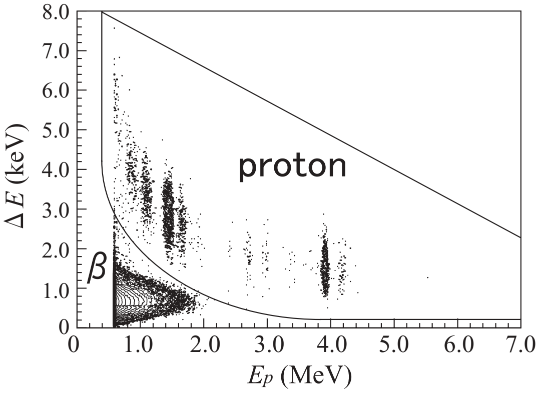

FIG. 6. Two-dimensional plot of ΔE-E. ΔE axis denotes a calculated value for the measured E_p. The delayed protons and β rays are clearly separated. The region framed by the solid line was projected to the E_p axis to generate Fig. 7.

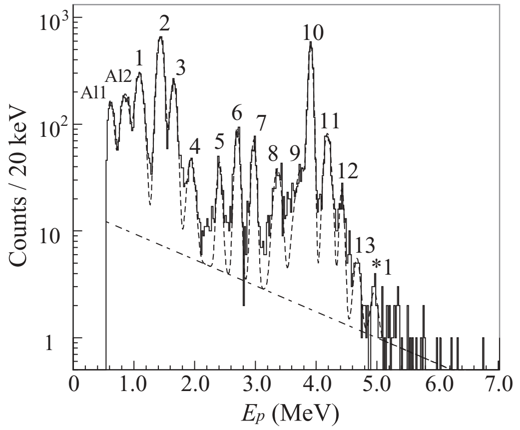

FIG. 7. Proton energy spectrum rejecting β rays. The dashed and the chain lines represent the fitting function and background, respectively. Proton peaks labeled as 1–13 originate from ^{24}Si, while Al1 and Al2 originate from ^{23}Al [27,32].

energy in comparison to the case of using reactions, with the value of the energy level revised to 1.090(1) MeV. The β transition to the 1.090-MeV level has a log(ft) value of 4.45, as will be shown in Sec. IV B, which is appropriate for an allowed transition. Due to the observation of the allowed β branch, it is possible to firmly establish the spin-parity for this level as 1^+.

The branching ratios to the 1^+_1 and 1^+_2 states were determined to be $b_1 = 0.31(4)$ and $b_2 = 0.239(15)$, respectively, by using the observables of the number of implanted ^{24}Si, the γ-line yields and the detection efficiency. A reference value for the electromagnetic transition ratio $I_\gamma(^{24}\mathrm{Al}^{\mathrm{m}}) = 0.82(3)$ [33] of the 1^+_1 isomeric state was used in the deduction of the b_1 value. The total branching ratio to the bound states is $b_\gamma = 0.55(4)$.

The determination of the branching ratio to the unbound states requires the combination of results for γ-ray and proton measurements. The total branching ratio to the unbound states is $b_{\mathrm{p}} = 0.45(4)$, which is the complement of b_γ. Furthermore, the absolute branching ratios b_{i} for the proton peaks were deduced in proportion to the relative intensities through renormalization with b_{p}, and the deduced values are shown in Table II. The uncertainty for b_{p} includes a systematic error of 3% for the total proton intensity, which stems from the probability of nonevaluated yields other than the identified peaks. The branching ratios for peaks 9, 12, and 13 were determined for the first time in this study.

The final states of the proton emission include not only the ground state, but also the excited states in ^{23}Mg. The observation of the delayed γ rays of 1.906 and 2.357 MeV originating from the β-proton decay of ^{24}Si, indicates decaying paths to the excited state at 2.357 MeV in ^{23}Mg. Peaks 3 and 4 were assigned to feed to the 2.357-MeV state based on the following two observations. First, the difference in reduced total decay energy $E_\mu = (24/23)E_p$ between pairs 3, 10, and 4, 11 is 2.357 MeV. Second, the sum of branching ratios for peaks 3 and 4, which amounts to 5.8(6)%, is in agreement with the γ-emitting branching ratio from the 2.357-MeV level, where $b_{2.357} = 4.8(6)\%$. In this estimation, it is assumed that the 1.906- and 2.357-MeV γ rays originate from ^{24}Si only, not ^{23}Al, since these two γ rays have half-lives of 139(11) ms, which is in good agreement with that of ^{24}Si. The other peaks, except for 3 and 4, were attributed to the transitions to the g.s. of ^{23}Mg, as shown in Table II. The same assumption has also been adopted in previous studies [18,19].

In determining the branching ratios, we assumed that the branch for the proton emission was equal to that of the β decay. If the isospin is a good quantum number, a proton emission from the isobaric analog state (IAS) is forbidden by the isospin selection rule. In the case of ^{24}Al, the 5.953-MeV level is the IAS, which has also been observed previously [16,18,19]. However, no γ rays from the IAS to a 1^+ state in ^{24}Al were observed in this experiment. Thus, the proton emission is the dominant decay mode in the IAS. The proton emission from the IAS is supposed to be induced by isospin mixing [34] with a 0^+ state with $T = 1$ near the IAS ($T = 2$).

The decay scheme of ^{24}Si as reconstructed in the present experiment is shown in Fig. 8.

B. Transition strength

The *ft* value is defined as the product of the partial half-life t_p and the integrated Fermi function f. The partial half-life t_p was deduced using the half-life $T_{1/2}$ and the branching ratios b. The half-life of ^{24}Si was determined to be $T_{1/2} = 140.5(15)$ ms, which is the weighted mean value of 140.1(26) ms from the γ-ray measurements and 140.8(18) ms from the proton measurements. The integrated Fermi function f was calculated in the same way as in [35], with $Q_{\mathrm{EC}} = 10.812(20)$ MeV in the Atomic Mass Table [14]. Electron capturing was ignored since its probability was estimated to be less than 10^{-3} of that of the β^+ decay. The deduced *ft* values are shown in Table III.

β-decay spectroscopy has an advantage for spin-parity assignment in terms of log(*ft*). The β decay of a proton-rich nucleus involves a super-allowed transition induced by the Fermi operator. In this case, the final state of the Fermi transition is the IAS with $J^\pi = 0^+$ and $T = 2$ [15–17]. In this experiment, log(*ft*) for the transition to the 5.953-MeV state is 3.07(3). Since such a small *ft* value indicates a superallowed transition, it was confirmed that the 5.953-MeV state was the IAS. On the other hand, it was possible to uniquely assign other final states to $J^\pi = 1^+$ due to the log(*ft*) values, which are appropriate for allowed transitions induced by the GT operator.

The superallowed transition to the 0^+ IAS is a pure Fermi transition due to the selection rule for the spin-parity. The expected *ft* value for the pure Fermi transition of $T_z = -2$ nuclei is 1.536×10^3 sec. In this experiment, the *ft* value for the superallowed transition to the IAS was determined to be $1.2(1) \times 10^3$ sec. Although the transition with the fastest *ft* value should be the one corresponding to the IAS, such an anomalously fast transition cannot be explained with the Fermi transition alone. The uncertainty for the *ft* value mainly stems from the error of the branching ratio, which amounts to 7%. Note that the branching ratio of 12.7(9)% to the IAS in this experiment is consistent with a previously obtained value of 12.8(9)% [18]. The reliability of other values contributing to the *ft* value should be considered. The error for Q_{EC} and E_{ex} is 20 keV [14] and 8 keV, respectively, generating a 3% error in the *ft* value. The Q_{EC} in Ref. [14] is a value compiled from [36–38], where the reference values are consistent with each other. Regarding the half-life, $T_{1/2} = 140.5(15)$ ms agrees well with previously obtained values [18,19], and the error (0.1%) is negligible in comparison to that induced by other factors. The factors used in the deduction of the *ft* value appear to be dependable. Therefore, the most probable cause is the resolution for proton peaks, where a degenerate 1^+ state might exist around the IAS. In this experiment, the peaks 3 and 10 were assigned to feed to the IAS. A proton emission following the Fermi transition should have a narrow natural width because of the isospin selection rule. For the peak 10, its width of 35 keV in rms is narrower than that of nearby peaks, therefore the peak 10 is supposed to originate from the Fermi transition. Around the peak 3, the energy resolution is spread as large as 100 keV (FWHM) because of energy losses. Although the peak 3 might include the GT component, we cannot claim the evidence for the peak overlapping from our experimental data.

The GT transition strengths B(GT) were deduced from the *ft* values. The *ft* value and B(GT) are related through the following equations:

$$B(\mathrm{GT}) = \frac{K}{(g_{\mathrm{A}}/g_{\mathrm{V}})^2 ft}, \tag{1}$$

with a constant $K = 6145$ sec and a coupling constant ratio $g_{\mathrm{A}}/g_{\mathrm{V}} = -1.266$ [39] of the vector and axial vector currents of the weak interaction. The deduced B(GT) are shown in Table III.

V. DISCUSSION

The mirror asymmetry of B(GT) reflects the changes in configuration in a proton-rich nucleus induced by a weakly bound s-wave proton. In this section, the B(GT) asymmetry is discussed by comparison with the mirror β-decay of ^{24}Ne. The changes in configuration accompanied by the TE shift is investigated on the basis of the B(GT) asymmetry. Subsequently, the B(GT) asymmetry is compared with theoretical calculations in order to clarify the contribution of weakly bound s-wave protons.

The deduced B(GT) of ^{24}Si were compared with those of its mirror nucleus ^{24}Ne [13]. In this paper, the B(GT) asymmetry is defined as the ratio $B(\mathrm{GT}^+)/B(\mathrm{GT}^-)$. The ratios were determined to be 0.78(11) and 0.90(8) for the 1_1^+ and 1_2^+ states, respectively. The B(GT) asymmetries appear in both the 1_1^+ and 1_2^+ states, although a large energy asymmetry is only seen in the 1_2^+ state. Rather, the asymmetry is larger in the 1_1^+ state than in the 1_2^+ state. The appearance of the B(GT) asymmetry in both states indicates changes in configuration. This is due to the fact that the energy asymmetry (the TE shift) is sensitive only to the s-orbital component, while the B(GT) asymmetry is sensitive to the changes in configuration mixing between the s- and the d-orbital components.

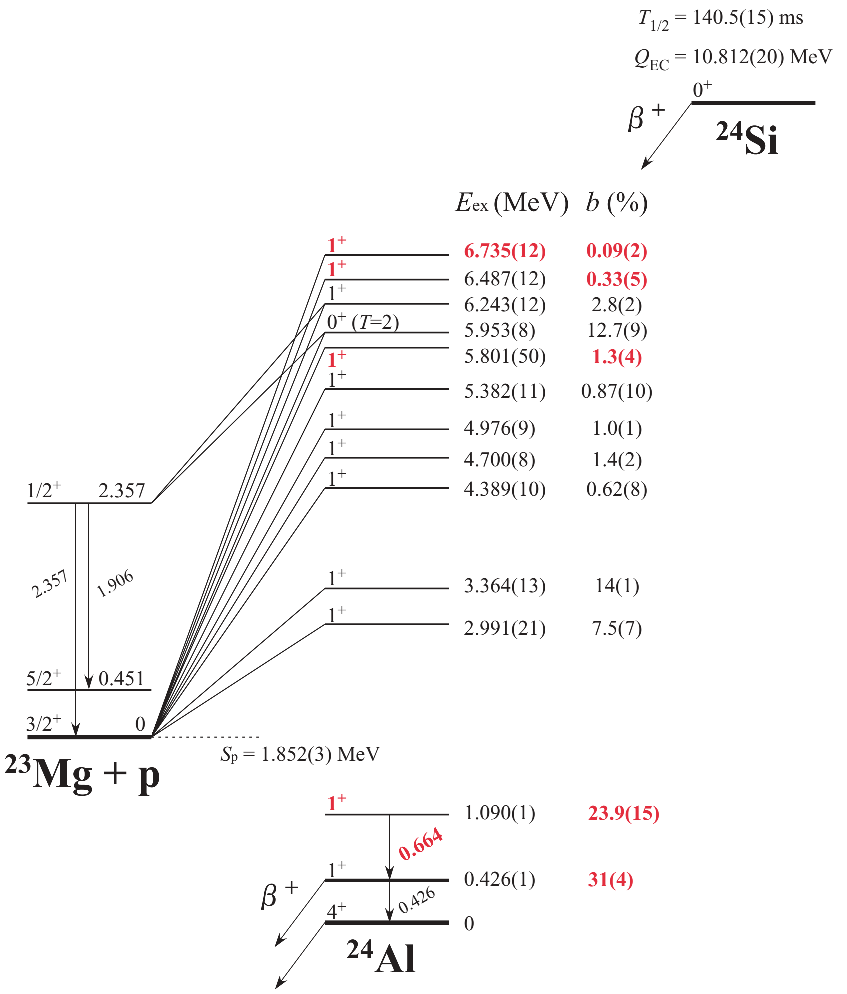

FIG. 8. (Color online) Decay scheme of ^{24}Si. Energy levels E_{ex}, branching ratios b and spin-parities J^π are denoted. Red (bold) characters denote the new values obtained in the present experiment.

To clarify the origin of the B(GT) asymmetry from a microscopic point of view, the experimental B(GT) were compared with the theoretical ones. The theoretical B(GT) were calculated in the sd-shell model space. The results for the B(GT) to the lowest two 1^+ states are given in Table IV for the USD [40] as well as the more recent USDA and USDB [41] Hamiltonians. These Hamiltonians are isospin-invariant, and the B(GT) values for the mirror decays are equal. The theoretical B(GT) were multiplied by 0.6 in order to take into account the empirical quenching [42], which can be attributed

TABLE III. Obtained branching ratio b, partial life t_p, ft value, and B(GT). Reference values for b and log(ft) are taken from Ref. [18]. The state of 5.953 MeV is the IAS of ^{24}Si.

E_{ex} (MeV)	b (%)	b [18] (%)	t_p (s)	ft (10^3 s)	log (ft)	log (ft) [18]	B(GT)
0.426(1)	31(4)		0.45(6)	31(4)	4.49(6)		0.13(2)
1.090(1)	23.9(15)		0.59(4)	28(2)	4.45(3)		0.14(1)
2.991(21)	7.5(7)	5.4	1.9(2)	28(3)	4.45(4)	4.61	0.14(1)
3.364(13)	14(1)	11.8	1.0(1)	12(1)	4.06(4)	4.16	0.34(3)
4.389(10)	0.62(8)	0.9	23(3)	120(10)	5.06(5)	4.94	0.03(1)
4.700(8)	1.4(2)	⩾1.4	10(1)	40(4)	4.60(5)	4.63	0.10(1)
4.976(9)	1.0(1)	⩾1.3	14(2)	41(5)	4.62(5)	4.55	0.10(1)
5.382(11)	0.87(10)	0.2	16(2)	32(4)	4.51(5)	5.18	0.12(2)
5.801(50)	1.3(4)		11(4)	14(5)	4.14(12)		0.28(9)
5.953(8)	12.7(9)	12.8(9)	1.10(8)	1.2(1)	3.07(3)	3.11	
6.243(12)	2.8(2)	3.8	5.1(4)	3.8(3)	3.57(4)	3.48	1.03(9)
6.487(12)	0.33(5)		42(6)	23(3)	4.36(6)		0.17(3)
6.735(12)	0.09(2)		160(40)	62(16)	4.79(10)		0.063(17)

TABLE IV. Comparison of experimental and theoretical Gamow-Teller strengths for the 1_1^+ and 1_2^+ states.

	^{24}Si $B(\mathrm{GT}^+,1_1^+)$	^{24}Si $B(\mathrm{GT}^+,1_2^+)$	^{24}Ne $B(\mathrm{GT}^-,1_1^+)$	^{24}Ne $B(\mathrm{GT}^-,1_2^+)$	Ratio (1_1^+) $B(\mathrm{GT}^+)/B(\mathrm{GT}^-)$	Ratio (1_2^+) $B(\mathrm{GT}^+)/B(\mathrm{GT}^-)$
Exp	0.13(2)	0.14(1)	0.167(4)	0.155(9)	0.78(11)	0.90(8)
USD	0.1077	0.1462	0.1077	0.1462	1	1
USDA	0.0665	0.1526	0.0665	0.1526	1	1
USDB	0.1231	0.1112	0.1231	0.1112	1	1
USD+C	0.1051	0.1353	0.1116	0.1450	0.94	0.93
USD+C*	0.0872	0.1418	0.1116	0.1450	0.78	0.98

to a combination of Δ-particle admixtures and configuration mixing outside the *sd* shell [43]. All three calculations are in reasonable agreement with the experiment, with USD and USDB being better than USDA for the 1_1^+ state.

Calculations for the mirror asymmetry were carried out with the Hamiltonian of Ormand and Brown [44], termed USD+C in Table IV. In addition to USD, this Hamiltonian contains the Coulomb interaction together with charge-independence breaking and charge-asymmetry breaking of strong interactions, where the strengths for the latter two were obtained empirically from a fit to the *b* and *c* coefficients of the isobaric mass multiplet equation. The use of USD+C results in some isospin asymmetry in the same direction as observed in the experiment.

The USD+C Hamiltonian does not account for the TE shift [1–3]. The occupancy of the $1s_{1/2}$ orbital is 0.445 for the 1_1^+ state and 0.834 for the 1_2^+ state in ^{24}Al. In addition, the one-proton separation energy for ^{24}Al is 1.87 MeV, while the one-neutron separation energy for ^{24}Na is 6.96 MeV [14]. Thus, the lowering of the energy of the 1_2^+ state in ^{24}Al relative to its position in the mirror ^{24}Na is indicative of a TE type shift. To take this into account, we repeated the USD+C calculation for the decay of ^{24}Ne by lowering the single-particle energy of the $1s_{1/2}$ proton orbital by 500 keV relative to the neutron single-particle energy. This lowers the energy of the 1_2^+ state in ^{24}Al by 202 keV as compared to the experimental shift of 256 keV. The ratio of the mirror B(GT) values is in good agreement with the experiment, as shown in the row corresponding to USD+C* in Table IV. The USD+C* as well as the USDB and USD+C Hamiltonians also provide a satisfactory reproduction of the overall B(GT) distribution covering the unbound states, as shown in Fig. 9. Thus, their applicability has been confirmed.

Details of the calculations for B(GT) are given in Table V for the decomposition of the matrix element M(GT) in terms of the contributions from various shell-model orbitals; $B(\mathrm{GT}) = Q|M(\mathrm{GT})|^2$, where $Q = 0.6$ is the quenching factor used in Table IV. The terms given in Table V are as follows:

$$M(\mathrm{GT}) = \sum_{j-j'} \mathrm{SPME}(j-j')\,\mathrm{OB}(j-j'), \qquad (2)$$

where SPME are the single-particle matrix elements and OB are the one-body transition densities [42].

For the results given in Tables IV and V, we used harmonic oscillator radial overlap factors of $\langle \pi, j \mid \nu, j\rangle = 1$ for the SPME. It is more realistic to calculate these overlaps with Woods-Saxon or Hartree-Fock single-particle wave functions. The overlaps obtained from the Skyrme Hartree-Fock calculation with SkX [45] for ^{24}Si (for orbitals with large occupation numbers) $\langle \pi, s_{1/2}|\nu, s_{1/2}\rangle = 0.983$ and $\langle \pi, d_{5/2}|\nu, d_{5/2}\rangle = 0.994$. Applying an SPME modification with these amounts induces insignificant changes in our results. More accurately, these radial overlap corrections

TABLE V. Details of transition densities to the 1_1^+ and 1_2^+ states. SPME and OB stand for single-particle matrix elements and the one-body transition densities [42].

$j-j'$	$0d_{5/2} \to 0d_{5/2}$	$0d_{5/2} \to 0d_{3/2}$	$0d_{3/2} \to 0d_{5/2}$	$0d_{3/2} \to 0d_{3/2}$	$1s_{1/2} \to 1s_{1/2}$	M(GT)
SPME$(j-j')$	2.898	−3.098	3.098	−1.549	2.449	
OB$(j-j')$; 1_1^+						
^{24}Ne USD	0.2866	0.0263	−0.1800	0.0074	0.0997	0.424
^{24}Ne USD+C	0.2862	0.0261	−0.1787	0.0074	0.1012	0.434
^{24}Si USD	0.2866	0.0263	−0.1800	0.0074	0.0997	0.424
^{24}Si USD+C	0.2855	0.0261	−0.1806	0.0072	0.0991	0.418
^{24}Si USD+C*	0.2619	0.0251	−0.1792	0.0094	0.1102	0.381
OB$(j-j')$; 1_2^+						
^{24}Ne USD	0.0827	−0.0229	0.0288	0.0068	0.0425	0.494
^{24}Ne USD+C	0.0812	−0.0231	0.0296	0.0068	0.0422	0.491
^{24}Si USD	0.0827	−0.0229	0.0288	0.0068	0.0425	0.494
^{24}Si USD+C	0.0819	−0.0201	0.0275	0.0071	0.0412	0.474
^{24}Si USD+C*	0.1097	−0.0109	0.0091	0.0107	0.0501	0.486

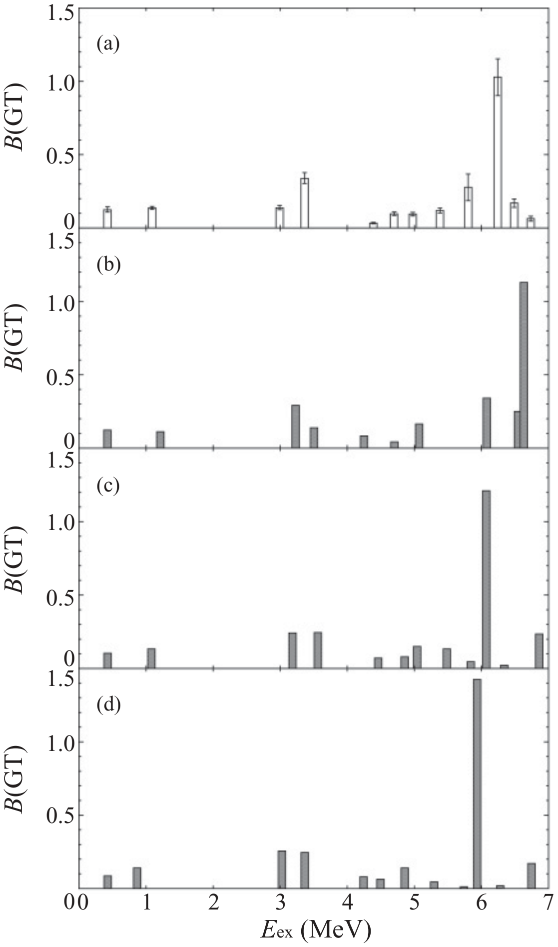

FIG. 9. B(GT) distributions corresponding to (a) the present experiment, (b) USDB, (c) USD+C, and (d) USD+C* calculations. In this figure, we exclude the possibility that the superallowed transition contains a GT component.

should be obtained in terms of an intermediate state expansion of the one-body transition densities [46]. However, given the small change in overlaps for our HF estimate, we do not expect the radial overlap correction to be notably large.

The origin of the mirror asymmetry is related to small differences in the various amplitudes of the one-body transition density, which have j to j' components that tend to cancel for the GT matrix elements to low-lying states. For the lowest 1^+ state, the $0d_{5/2} \rightarrow 0d_{5/2}$ and $1s_{1/2} \rightarrow 1s_{1/2}$ amplitudes are in phase, while they are largely canceled by the $0d_{5/2} \rightarrow 0d_{3/2}$ contribution. The main effect of lowering the $1s_{1/2}$ proton orbital is the weakening of the contribution from $0d_{5/2} \rightarrow 0d_{5/2}$ by 6%, where the total matrix element is 12% smaller (and the B(GT) is 22% smaller) than that in the mirror nucleus. The one-body transition densities to the 1_2^+ state are significantly modified by the lowering of the $0s_{1/2}$ orbital, while accidentally the total sum is not changed notably.

VI. SUMMARY

We carried out β-decay spectroscopy of the proton-rich nucleus ^{24}Si consisting of delayed-γ-ray measurements carried out for the first time, as well as delayed proton measurements employing an upgraded ΔE-E method to obtain large statistics. The decay scheme of ^{24}Si was reconstructed by combining the results from the two measurements. Two β transitions to the low-lying bound states in ^{24}Al were observed for the first time. The branching ratios to the 1_1^+ state at 0.426 MeV and a state at 1.090 MeV were determined to be 31(4)% and 23.9(15)%, respectively. Based on the observation of an allowed β branch, the spin-parity of the 1.090-MeV state was firmly determined to be 1^+. For unbound states, we observed a new level at 6.375 MeV in ^{24}Al and determined three branching ratios for the first time. The previously observed proton peaks [18,19] were confirmed to originate from ^{24}Si.

The B(GT) values of ^{24}Si were deduced for the observed allowed transitions. By comparing the B(GT) values with its mirror counterpart, the ratios were derived to be 0.78(11) and 0.90(8) for the 1_1^+ and 1_2^+ states, respectively, where a TE shift was observed. The B(GT) asymmetries, which were observed not only in the 1_2^+ state, but also in the 1_1^+ state, indicate changes in configuration in the wave function associated with the TE shift. To clarify the mechanism of the asymmetry from a microscopic perspective, the experimental values were compared with theoretical estimates obtained with the shell model. The experimental B(GT) asymmetries were reproduced by the shell-model calculation with effects of the weak binding energy, where the single particle energy of the $1s_{1/2}$ orbital is lowered to reproduce the TE shift for the 1_2^+ state in ^{24}Al. The applicability of the calculation was confirmed in terms of the overall B(GT) distribution. The calculation attributed the B(GT) asymmetry in the 1_1^+ state to the changes in configuration associated with the lowering of the $1s_{1/2}$ orbital. For the 1_2^+ state, the changes in some amplitudes are canceled, and in those cases the B(GT) asymmetry is not significant.

ACKNOWLEDGMENTS

This experiment was carried out under Program No. R365n at RIKEN Accelerator Research Facility operated by RIKEN Nishina Center and CNS, University of Tokyo. We thank the RIKEN Ring Cyclotron staff for their cooperation during the experiment. We also thank Prof. A. Gelberg for a careful reading of the manuscript. Y.I. is grateful to the Junior Research Associates Program and the Special Postdoctoral Researchers Program in RIKEN. This work was supported in part by a Grant-in-Aid for Scientific Research No. 15204017 in Japan, an NSF Grant PHY-0758099 in the USA, and the Japan-US Theory Institute for Physics with Exotic Nuclei (JUSTIPEN).

---

[1] R. G. Thomas, Phys. Rev. **88**, 1109 (1952).
[2] J. B. Ehrman, Phys. Rev. **81**, 412 (1951).
[3] A. Bohr and B. R. Mottelson, *Nuclear Structure*, Vol. I (W. A. Benjamin, New York, 1969).

[4] K. Ogawa *et al.*, Phys. Lett. **B464**, 157 (1999).
[5] L. V. Grigorenko, I. G. Mukha, I. J. Thompson, M. V. Zhukov, Phys. Rev. Lett. **88**, 042502 (2002).
[6] X. Z. Cai *et al.*, Phys. Rev. C **65**, 024610 (2002).
[7] A. Ozawa *et al.*, Phys. Rev. C **74**, 021301(R) (2006).
[8] K. Asahi, K. Matsuta, K. Takeyama, K. H. Tanaka, Y. Nojiri, T. Minamisono, Phys. Rev. C **41**, 358 (1990).
[9] B. J. G. Borge *et al.*, Phys. Lett. **B317**, 25 (1993).
[10] A. J. Armini *et al.*, Phys. Lett. **21**, 335 (1966).
[11] G. C. Kiang *et al.*, Nucl. Phys. **A499**, 339 (1989).
[12] S. Kubono *et al.*, Nucl. Phys. **A588**, 521 (1995).
[13] R. E. McDonald *et al.*, Phys. Rev. **181**, 1631 (1969).
[14] G. Audi *et al.*, Nucl. Phys. **A729**, 337 (2003).
[15] J. Äystö *et al.*, Phys. Lett. **B82**, 43 (1979).
[16] J. Äystö, M. D. Cable, R. F. Parry, J. M. Wouters, D. M. Moltz, J. Cerney, Phys. Rev. C **23**, 879 (1981).
[17] A. G. Ledebuhr, L. H. Harwood, R. G. H. Robertson, T. J. Bowles, Phys. Rev. C **22**, 1723 (1980).
[18] S. Czajkowski *et al.*, Nucl. Phys. **A628**, 537 (1998).
[19] V. Banerjee *et al.*, Phys. Rev. C **63**, 024307 (2001).
[20] T. Kubo *et al.*, Nucl. Instrum. Methods Phys. Res. B **70**, 309 (1992).
[21] H. Kumagai *et al.*, Nucl. Instrum. Methods Phys. Res. A **470**, 562 (2001).
[22] D. M. Moltz *et al.*, Nucl. Instrum. Methods Phys. Res. A **349**, 210 (1994).
[23] T. K. Onishi *et al.*, Phys. Rev. C **72**, 024308 (2005).
[24] P. M. Endt *et al.*, Nucl. Phys. **A521**, 1 (1990).
[25] V. S. Shirley *et al.*, *Table of Isotopes*, Vol. 1 (Wiley Interscience, New York, 1996).
[26] V. E. Iacob *et al.*, Phys. Rev. C **74**, 045810 (2006).
[27] K. Peräjärvi *et al.*, Phys. Lett. **B492**, 1 (2000).
[28] J. C. Hardy *et al.*, Phys. Rev. Lett. **91**, 082501 (2003).
[29] GEANT4: Detector Description and Simulation Tool, CERN Program Library.
[30] V. E. Iacob *et al.*, Phys. Rev. C **74**, 015501 (2006).
[31] R. G. Sextro *et al.*, Phys. Rev. C **8**, 258 (1973).
[32] R. A. Gough *et al.*, Phys. Rev. Lett. **28**, 510 (1972).
[33] J. Honkanen *et al.*, Phys. Scr. **19**, 239 (1979).
[34] B. A. Brown, Phys. Rev. Lett. **65**, 2753 (1990).
[35] D. H. Wilkinson *et al.*, Nucl. Phys. **A232**, 58 (1974).
[36] R. E. Tribble, D. M. Tanner, A. F. Zeller, Phys. Rev. C **22**, 17 (1980).
[37] G. R. Burleson *et al.*, Phys. Rev. C **22**, 1180 (1980).
[38] H. Schatz *et al.*, Phys. Rev. Lett. **79**, 3845 (1997).
[39] K. Schreckenbach *et al.*, Phys. Lett. **B349**, 427 (1995).
[40] B. A. Brown and B. H. Wildenthal, Annu. Rev. Nucl. Part. Sci. **38**, 29 (1988).
[41] B. A. Brown and W. A. Richter, Phys. Rev. C **74**, 034315 (2006).
[42] B. A. Brown and B. H. Wildenthal, At. Data Nucl. Data Tables **33**, 347 (1985).
[43] B. A. Brown and B. H. Wildenthal, Nucl. Phys. **A474**, 290 (1987).
[44] W. E. Ormand and B. A. Brown, Nucl. Phys. **A491**, 1 (1989).
[45] B. A. Brown, Phys. Rev. C **58**, 220 (1998).
[46] I. S. Towner, Nucl. Phys. **A216**, 589 (1973).